Biosensors and Bioelectronics 59 (2014) 140–144

Contents lists available at ScienceDirect

Biosensors and Bioelectronics

journal homepage: www.elsevier.com/locate/bios

Planar Hall magnetoresistive aptasensor for thrombin detection

B. Sinha [a], T.S. Ramulu [a,b], K.W. Kim [a,b], R. Venu [a,b], J.J. Lee [c], C.G. Kim [a,b,*]

[a] Department of Materials Science and Engineering, Chungnam National University, Daejeon 305-764, South Korea
[b] Department of Emerging Materials, Daegu Gyeongbuk Institute of Science and Technology, Daegu 711-873, South Korea
[c] Nano-Mechanical Systems Research Division, Korea Institute of Machinery & Materials, Daejeon 305-600, South Korea

ARTICLE INFO

Article history:
Received 13 December 2013
Received in revised form
4 March 2014
Accepted 11 March 2014
Available online 27 March 2014

Keywords:
Planar Hall magnetoresistive sensor
Aptasensor
Thrombin
Sandwich

ABSTRACT

The use of aptamer-based assays is an emerging and attractive approach in disease research and clinical diagnostics. A sensitive aptamer-based sandwich-type sensor is presented to detect human thrombin using a planar Hall magnetoresistive (PHR) sensor in cooperation with superparamagnetic labels. A PHR sensor has the great advantages of a high signal-to-noise ratio, a small offset voltage and linear response in the low-field region, allowing it to act as a high-resolution biosensor. In the system presented here, the sensor has an active area of 50 μm × 50 μm with a 10-nm gold layer deposited onto the sensor surface prior to the binding of thiolated DNA primary aptamer. A polydimethylsiloxane well of 600-μm radius and 1-mm height was prepared around the sensor surface to maintain the same specific area and volume for each sensor. The sensor response was traced in real time upon the addition of streptavidin-functionalized magnetic labels on the sensor. A linear response to the thrombin concentration in the range of 86 pM–8.6 μM and a lower detection limit down to 86 pM was achieved by the proposed present method with a sample volume consumption of 2 μl. The proposed aptasensor has a strong potential for application in clinical diagnosis.

1. Introduction

The detection of protein that binds with sequence-specific DNA (Aptamer) plays a significant role in disease research and clinical diagnosis, due to the long term stability of the probe DNA. In molecular biology, thrombin is one of the important proteins because, through its concentration, thrombin performs a crucial role in physiological and pathological conditions (Zhang and Sun, 2011) particular, thrombin is one of the target biomarkers for cardiovascular disease, being essential to several coagulant effects as well as acting as a useful tumor marker for the diagnosis of pulmonary metastasis (Edwards et al., 2010, Nierodzik and Karpatkin, 2006, Yoon et al., 2013). Therefore, the development of the devices for the monitoring and detection of thrombin with high sensitivity and selectivity is of enormous importance in medical applications.

DNA aptamers are single-stranded (ss) DNA, which bind to their target molecules with high affinity, specificity and stability that act as model diagnostic in vitro reagents and are potential replacements for antibody biomarkers in the use of nanobiotechnology in biomolecular sensors (Cho et al., 2008, Qiu et al., 2010, Zhang and Sun, 2011, Shimada et al., 2012, Xu et al., 2006). DNA aptamers exhibit several superior properties compared to antibodies, such as long-term and thermal stability, inexpensive production, consistent chemical synthesis, labeling and selective changes in sequences (Cho et al., 2008, Edwards et al., 2010, Yang et al., 2009). As a result, the development of aptamer-based detection methods has received great interest for use in detection of thrombin. Hence, various types of DNA-aptamer based techniques have been used, including fluorescence, surface plasma resonance, quartz crystal microbalance and electrochemistry, for thrombin detection (Lu et al., 2009, Bai et al., 2013; Chen et al., 2010, Fan et al., 2012).

Magnetic labels coupled with magnetoresistive (MR) sensors can detect very low bio-molecules concentrations and have an extensive linear dynamic range compared with the above mentioned detection methods (Oh et al., 2013). In addition, other compounds present in the investigated samples do not exhibit any magnetic behavior, consequently minimizing the noise and possible interference of foreign substances in the MR signal measurements (Larsson et al., 1999). Hence, the development of MR sensors is significantly increasing towards bio-applications in both industrial and basic academic research as well as for point-of-care diagnostics. Moreover, MR sensors are low-power consumuption devices that are highly sensitive, easily scalable, inexpensive and portable (Oh et al., 2013). Several types of MR sensors, such as

* Corresponding author at: Department of Emerging Materials, Daegu Gyeongbuk Institute of Science and Technology, Daegu, 711-873, Republic of Korea. South Korea. Tel.: +82537856516; fax: +82537856509.
E-mail address: cgkim@dgist.ac.kr (C.G. Kim).

http://dx.doi.org/10.1016/j.bios.2014.03.021
0956-5663/

semiconductor Hall sensor (Besse et al., 2002), anisotropic magnetoresistive (AMR) (Miller et al., 2002), giant magnetoresistive (GMR) (Baselt et al., 1998, Ferreira et al., 2003, Mak et al., 2010), tunneling magnetoresistive (TMR) (Albisetti et al., 2013) and giant magneto-impedance (GMI) (Kurlyandskaya and Levit, 2005; Yang et al., 2010) sensors, have been reported in the field of bio-sensing applications. Although PHR sensors have great advantages of high signal-to-noise ratio, small offset voltage at zero field and very linear response in the low field region (Sinha et al., 2013, Hung et al., 2010, Sinha et al., 2012), biosensing application of PHR sensors for molecular diagnostics has not been reported yet.

In this study, we report the development of a sensitive aptamer-based PHR sensor for human α-thrombin detection. The sensing mechanism is based on the sandwich-type aptamer assay. The sensor surface was modified with thiol-labeled primary aptamer, and then thrombin was applied to the aptamer immobilized surface. After that, biotin-labeled secondary aptamer was used to bind with thrombin. Finally, streptavidin-coated magnetic nanoparticles were used to measure the MR signal. The MR signal was measured by the changes in the thrombin concentration which results in the changes in the amount of biotin-labeled secondary aptamer for the binding of streptavidin-coated magnetic nanoparticles in the assay.

2. Materials and methods

2.1. Materials and chemicals

The sputtering targets of $Ni_{80}Fe_{20}$, Ta, $Ir_{25}Mn_{75}$, Cu, Au and SiO_2 with a purity of 99.99% were procured from Kojundo Chemical Laboratory Co. Ltd., Japan, and used to fabricate the PHR sensor. The SiO_2 substrates were purchased from Wafermart, Korea. The Photoresist (PR) AZ 5214E and Developer AZ 500MIF were purchased from AZ Electronic Materials USA Corp. The epoxy (PT-135K) was obtained from Poly-tech Co. Ltd. Korea. Streptavidin functionalized magnetic nanoparticles embedded in starch with an average size of 100 nm were procured from Chemicell GmbH, Germany. Phosphate buffered saline (PBS, pH 7.4) was purchased from Bioneer Corporation, Korea. Tris-EDTA buffer (pH 8.0) and human α-thrombin were obtained from Sigma-Aldrich. All of the oligonucleotides (aptamers) were purchased from GeneChem Inc, Korea with a thiol modified 15–mer primary aptamer with a poly tail of thymine and a biotinylated 15-mer secondary aptamer. The base sequences used in this study are as follows:

1. Thiolated primary aptamer: 5′-SH– $(CH_2)_6$-TTTTTTTTTTTTTT GGT TGG TGT GGT T GG-3′
2. Biotinylated secondary aptamer: 5′-biotin-GGT TGG TGT GGT TGG-3′

The primary aptamer is specific to fibrinogen binding site of the thrombin. This specific binding site is formed by the sequence GGT TGG TGT GGT TGG (Porfirieva et al., 2007), while the rest part of the aptamer is essential for its proper binding to the sensor surface.

2.2. Sensor fabrication

The cross-junction PHR sensors with an arm length of 100 μm and an active junction area of 50 μm × 50 μm were prepared on SiO_2 substrates using standard UV photolithography. Here, the sensor patterning was performed by photolithography using a spin coater (Spin-1200D, Midas System Co. Ltd. Korea) and a mask aligner (MDA–400s, Midas System Co. Ltd. Korea). In briefly, the SiO_2 substrate was cleaned in methanol and acetone solution using an ultrasonic cleaner for 30 min and dried using N_2 gas. Then, the substrate was coated with PR using a spin coater at 3000 rpm for 30 s. The PR thickness was ~1.6 μm, and soft baking was performed for 1 min at 120 °C to enhance the adhesion of the PR layer. The photolithography process is shown in Fig. S1, which used a Cr mask pattern aligned by a mask aligner, was used to form a sensor junction onto the PR coated substrate. After UV exposure, the PR layer was developed and rinsed with DI water, and the substrate was dried using N_2 gas. Then, a trilayer structure of thin films of Ta/NiFe/Cu/IrMn/Ta (3/10/0.26/10/3 nm) was sequentially deposited onto the substrate by using a DC magnetron sputtering system (Daeki hi-Tech. co. Ltd., Korea) under the working pressure of 3 mTorr with a base pressure of $\sim 1.0 \times 10^{-7}$ Torr. During the sputtering process, a uniform magnetic field of 200 Oe was applied parallel to the film plane to induce a magnetic anisotropy of ferromagnetic (FM) layer and to align the pinning direction of the antiferromagnetic (AFM) IrMn layer, which fixed the easy axis of the sensor to the field direction.

After the deposition of the multilayer thin film, the PR was removed using acetone and methanol and dried using a flow of N_2. Next, using a similar photolithography process and DC magnetron sputtering to those described above, Ta/Au (10/50 nm) electrodes were prepared to connect sensor junctions to the PCB. After that, the sensor junctions and electrodes were passivated with a SiO_2 (100 nm) layer deposited using RF magnetron sputtering to protect the sensor junctions and electrodes from corrosion in the fluidic environment during the experiment. Finally, an Au (10 nm) film was deposited using the above mentioned photolithography on the sensor surface for binding the thiolated aptamer to the sensor. The SiO_2 substrate containing the sensors was attached to the PCB. The sensors and the PCB were connected by using Au micro-wire bonding (7476D, West Bond Inc. USA), and the electrical connection was protected by coating it with epoxy. More details of the sensor fabrication process are described elsewhere (Hung et al., 2010).

2.3. Characterization of the magnetic labels and the sensor

Sensor characterization and measurements were performed using a function generator (HP/Agilent 8116A 50 MHz Programmable Pulse/Function Generator, USA) and a magnetic field generator (RPA–2A, www.magsen.com) prior to a hand-made Helmholtz coil and a Lock-In amplifier (SR830DSP; Stanford Research Systems, USA). The morphology of the magnetic nanoparticles was characterized using a field-emission scanning electron microscope (FE-SEM, Magellan400, FEI Company) at an operating voltage of 2 kV, and the magnetic properties were measured using a vibrating sample magnetometer at room temperature (VSM, Lakeshore 7407 series) with a sensitivity of 10^{-6} emu. The VSM measurement of the magnetic labels was done by drying the magnetic labels.

2.4. Sandwich structure of thrombin using aptamer on the sensor surface

In this study, thrombin was sandwiched between two aptamers, one covalently bound to Au on the sensor surface (primary aptamer) and the other bound to the target thrombin with biotin (secondary aptamer). A scheme of the detection of thrombin is shown in Fig. 1. The sensor chip was cleaned using methanol, followed by rinsing with distilled water, and then was dried by a gentle flow of N_2. Immobilization of thiolated 15-mer primary aptamer on the Au-covered sensor surface was followed by application of 5 μL of 70–ng/μl primary aptamer solution in Tris-EDTA buffer into the reaction well, which was allowed to sit overnight, allowing it to form Au–S bond with Au surface. Subsequently, the well was washed with Tris–EDTA buffer to remove any unbound aptamer. Then, for each sample studied, 2 μL of

the appropriate concentration (8.6 μM to 86 pM with a 10 × dilution) of thrombin was added to the primary aptamer immobilized sensor surface, followed by incubation for 1 h at 37 °C, during which time thrombin was captured onto aptamer/Au sensor surface. After that, the well was washed using PBS buffer to remove the unbound thrombin. Finally, 5 μL of 70–ng/μl biotinylated 15–mer secondary aptamer solution was added to complete the sandwich structure, which was incubated for 1 h at 37 °C. The sensors were then washed again with Tris-EDTA buffer and kept at 4 °C for further magnetic measurements.

3. Results and discussion

The morphology of the magnetic nanoparticles shown in Fig. 2(a) was observed using the FE-SEM. The mean diameter of the magnetic nanoparticles were found to be approximately 100 nm, which resembles the data provided by the manufacturer. It is seen from the image that the nanoparticles are well dispersed in solvent. For more clear observation, the image of a single nanoparticle is shown in the figure inset. The physiochemical properties of streptavidin-coated magnetic labels are summarized in Table S1 (please see the Supplementary information).

Fig. 2(b) shows the *M–H* curve of the magnetic nanoparticles. The hysteresis loop was measured within a ± 1.0 kOe applied magnetic field. The magnetization was approximately 45 emu/g at 1 kOe, while the magnetization value at 100 Oe was 15 emu/g. The inset shows a low-field *M–H* curve, which indicates the linear response with the field and superparamagnetism behavior, with rapid response to the applied magnetic field. The magnetic labels exhibit negligible remanence (~2 Oe) and coercivity (~2 Oe), and their magnetic susceptibility was calculated to be 0.95 (SI) in the low-field region.

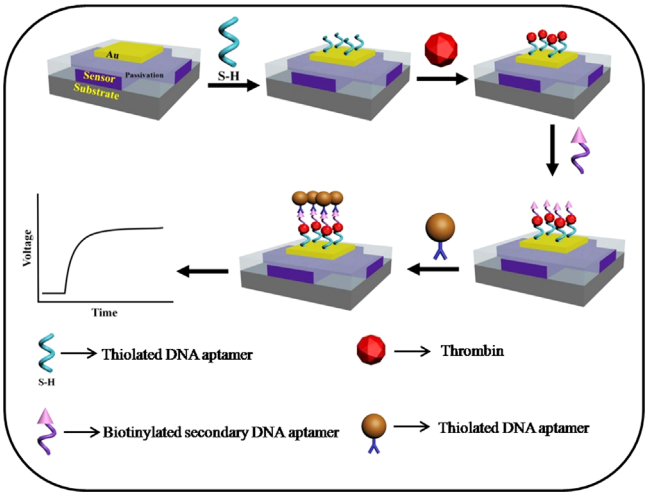

Fig. 1. Schematic representation of the aptamer-based thrombin detection using PHR sensors.

The sandwiched structure, aptamer/thrombin/aptamer modified sensor was placed in the Helmholtz coil for the signal measurement. A block diagram of the measurement set up is shown in the Supplementary information (Fig. S2). Here, the direction of the sensing current for the sensor was set along the easy axis of the sensor and is perpendicular to the magnetic field direction. The voltage of the sensor was measured along the magnetic field direction. A magnetic field of 113 Hz with a magnitude of 15 Oe was applied to the sensor. The sensor voltage was measured by using a Lock-In amplifier with a 1*f* mode through Lab–View program control, and the signal was averaged over 30 points.

A polydimethylsiloxane (PDMS) reaction well of 600-μm radius and 1-mm height was prepared around the sensor surface to maintain the same specific area and volume for each of the sensors. The picture of the prototype sensor with PDMS well is shown in Fig. 3(a). For more clear understanding of the sensor and the PDMS well, a high magnification schematic image of the sensor region is shown in Fig. 3(b)

Each measurement was initiated when the sensor surface was free of solution to ensure sensor stability and to establish a signal base line. A small shift of the baseline was rarely observed due to the wet/dry transitions and was negligible compared to the magnitude of the signals of interest. The signal was usually stabilized within 1 min. Once a signal baseline was established, 10 μL of streptavidin-coated magnetic label solution was added to the reaction well. The system remained unstirred during the measurement at room temperature. The measurements were terminated when the signal level was stabilized, usually within 10 min. The unbounded particles are sucked by tissue paper inserted into the PDMS well very gently away from the sensor area without mechanical touching.

A typical magnetic label binding curve with the target is schematically shown in Fig. 4(a). The superparamagnetic labels become magnetized when the external magnetic field is applied through the Helmholtz coil. Their presence in close proximity of the PHR sensor surface alters the local magnetic field and consequently changes the voltage of the sensor. The magnetic labels were added to the reaction well after establishing a baseline in voltage (Fig. 4a, portion–I). The binding of the magnetic label to the biotinylated aptamer with thrombin occurs immediately upon contact and causes the change of the sensor signal in real time (Fig. 4a, portion–II). Note that the signal is caused by the streptavidin–biotin binding rather than aptamer–thrombin binding. The available binding sites for the magnetic labels are a function of the thrombin added before the incubation of the biotinylated secondary aptamer. Therefore, the stabilized level of the signal along with the magnetic labels binding is taken as a direct indication of the thrombin concentration. Typically, the

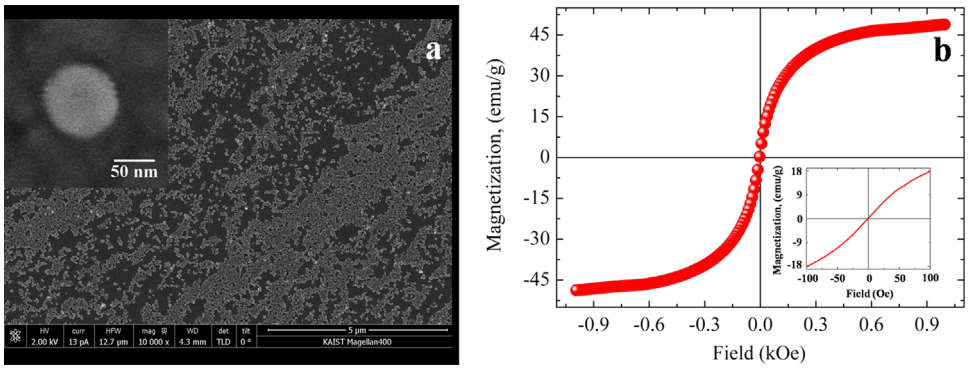

Fig. 2. Scanning electron microscope image of the magnetic labels (the inset shows an individual nanoparticle) (a) and *M–H* curve for magnetic labels (b).

signal level becomes constant (Fig. 4a, portion–III) when the thrombin binding sites are not available, and the absolute values of the signal change are used for data analysis and comparison purposes.

Two comparative experiments were performed by incubating the aptasensor without and with thrombin of 8.6-μM concentration, and the resulting experimental curves are shown in Fig. 4(b). The data clearly reveals that the binding of magnetic labels occurred immediately on the sensor where thrombin was sandwiched. After 3 min, the signal level becomes constant, with a signal change of approximately 41.5 μV. Meanwhile, the other sensor, which was not expected to show any interaction, gave a negligible signal corresponding to the system noise value. The result confirmed the binding specificity of the thrombin to the aptamers.

Various concentrations of thrombin and their corresponding real-time measured signals are shown in Fig. 4(c). A series of thrombin concentrations were used, ranging from 8.6 μM to 86 pM. From Fig. 4(c), it is clearly seen that the change of the sensor output signal is sensitive to the thrombin concentration, and an increase of thrombin in concentration leads to an increased sensor signal. Moreover, the response of the sensor signal was rapid for the higher concentration of thrombin, whereas the response was slower for the lower concentration. In addition, the sensor signal become constant quite rapidly at the high concentration compared to the response at the lower concentration (pM). This behavior is due to the large number of binding sites of thrombin for biotinylated secondary aptamer for the higher concentration of thrombin. Ultimately, the large number of biotinylated secondary aptamer could be coupled with magnetic labels within a short period of time, resulting in the high affinity of biotin–streptavidin for the high concentration. Although the signal for 86 pM appears to be the baseline response, the output voltage of approximately 0.6 μV is a significant value. For clarity, signals for the 86-pM and 0.86-nM curves are shown in Fig. 4(d) with an enlarged scale.

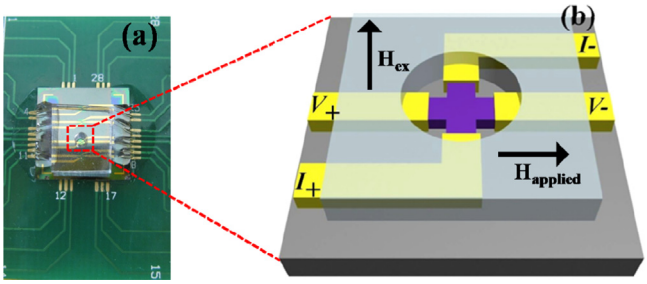

Fig. 3. PHR sensor prototype (a). Schematic of the PHR sensor (b).

The linear relationships between the sensor output signal and the logarithms of the thrombin concentration over a range of 86 pM to 8.6 μM are shown in Fig. 5. The maximum change in the output voltage for all concentrations over 8 min was chosen. Even though there is some deviation in low concentration region below 8.6 nM, as whole the signal voltage change exhibited a good linear relationship with the logarithm of the thrombin concentration, which obeys the following Eq. (1) with a regression coefficient of 0.983.

$$\Delta V(\mu V) = 8.36 \times \log \times M_{\text{thrombin}} + 0.82 \times 10^2 \quad (1)$$

M_{thrombin} = Molar concentration of thrombin

The minimum concentration detection of 86 pM was achieved with this MR aptasensor, which is lower than those of glass surface functionalization for aptamer immobilization (Huang et al., 2010)

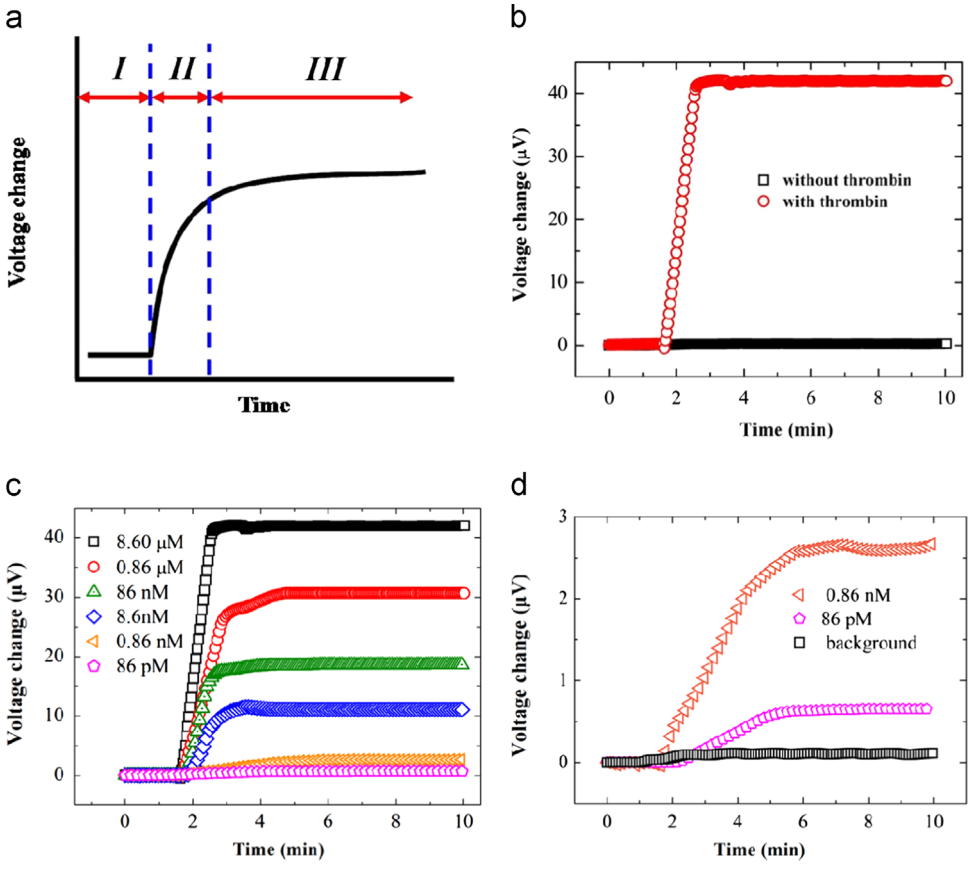

Fig. 4. Schematic illustration of the typical PHR voltage for magnetic labels binding (a). Specificity of the aptamer without and with a thrombin concentration of 8.6 μM (b). Real-time PHR signal monitoring for different thrombin concentrations (c). High magnification signal curve for 86-pM and 0.86-nM concentrations (d).

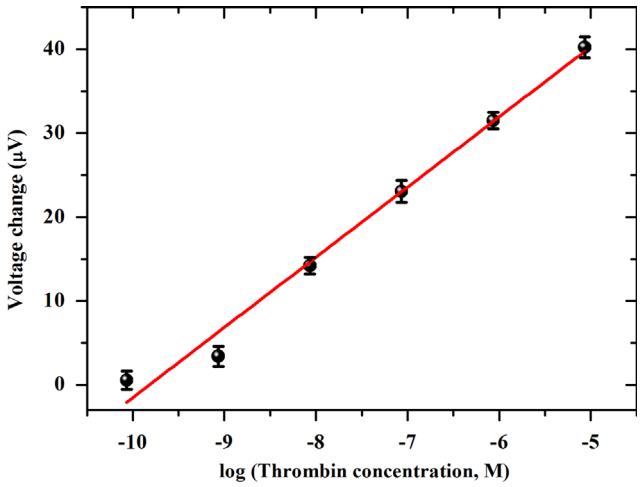

Fig. 5. Change of the PHR signal as a function of the logarithm of the thrombin concentration, ranging from 86 pM to 8.6 μM.

Table 1
Detection limit of thrombin using different measurement strategies.

Sl. no	Method of detection	Detection Limit	References
1	Fluorescence	7.7 nM	Huang et al. (2010)
2	Surface plasma resonance	11 nM	Shimada et al. (2012)
3	Colorimetric	1 nM	Liang et al. (2011)
4	Electrochemical	0.1 nM	Feng et al. (2013)
5	Quartz crystal microbalance	0.1 nM	Chen et al. (2010)
6	Magnetic method	86 pM	Present study

and those of the use of DNA-enzyme (Shimada et al., 2012), gold coated Fe_3O_4 nanoparticles (Liang et al., 2011), gold nanoneedles (Feng et al., 2013) and gold nanoparticles (Chen et al., 2010). The details of the measurement methods and the detection limit are listed in Table 1. This analysis suggests that the PHR aptasensor is a high-resolution biosensor for diagnosis of diseases and is useful for detection of many other proteins. The reproducibility experiment was performed for various concentrations of thrombin by measuring the real time signal. The average change in output voltage and standard deviation is shown in Table S2 (Supplementary information).

4. Conclusion

A novel PHR aptasensor has been developed for the detection of thrombin in cooperation with superparamagnetic labels, and the aptamer/thrombin/aptamer sandwich model was successfully used for this PHR sensor. Two thrombin-binding aptamers individually bind to the target thrombin molecule formed by sandwich aptamer complexes. This PHR aptasensor achieves a detection limit of a thrombin concentration of 86 pM. The performed PHR aptasensor may be a good candidate for the clinical diagnosis of thrombotic diseases. Moreover, the PHR sensor may be useful for the fabrication of DNA sensors and immunosensors.

Acknowledgments

This work was supported by SMBA 2012 program (C0021020) and BioNano Health-Guard Research Center funded by the Ministry of Science, ICT & Future Planning (MSIP) of Korea as Global Frontier Project (Grant number H-GUARD_2013M3A6B2078)

Appendix A. Supporting information

Supplementary data associated with this article can be found in the online version at http://dx.doi.org/10.1016/j.bios.2014.03.021.

References

Albisetti, A., Petti, D., Cantons, M., Damin, F., Torti, A., Chiari, M., Bertacco, R., 2013. Biosens. Bioelectron. 47, 213–217.
Bai, Y., Fenga, F., Zhao, L., Wang, C., Wang, H., Tian, M., Qin, J., Duan, Y., He, X., 2013. Biosens. Bioelectron. 47, 265–270.
Baselt, D.R., Lee, G.U., Natesan, M., Metzger, S.W., Sheehan, P.E., Colton, R.J., 1998. Biosens. Bioelectron. 13, 731–739.
Besse, P.-A., Boero, G., Demierre, M., Pott, V., Popovic, R., 2002. Appl. Phys. Lett. 80, 4199.
Chen, Q., Tang, W., Wang, D., Wu, X., Li, N., Liu, F., 2010. Biosens. Bioelectron. 26, 575–579.
Cho, H., Baker, B.R., Hogiu, S.W., Pagba, C.V., Laurence, T.A., Lane, S.M., Lee, L.P., Tok, J.B.-H., 2008. Nano Lett. 8, 4386–4390.
Edwards, K.A., Wang, Y., Baeumner, A.J., 2010. Anal. Bioanal. Chem. 398, 2645–2654.
Fan, H., Li, H., Wang, Q., He, P., Fang, Y., 2012. Biosens. Bioelectron. 35, 33–36.
Feng, X., Mei, H., Huai, D., Yunhui, Y., 2013. J. Nanosci. Nanotechnol. 13, 558–563.
Ferreira, H.A., Graham, D.L., Freitas, P.P., Cabra, J.M.S., 2003. J. Appl. Phys. 93 (10), 7281.
Huang, D.-W., Niu, C.-G., Qin, P.-Z., Ruan, M., Zeng, G.-M., 2010. Talanta 83, 185–189.
Hung, T.Q., Oh, S., Sinha, B., Jeong, J.-R., Kim, D.-Y., Kim, C.G., 2010. J. Appl. Phys. 107 (9), 09E715.
Kurlyandskaya, G., Levit, V., 2005. Biosens. Bioelectron. 20, 1611–1616.
Larsson, K., Kriz, K., Kriz, D., 1999. Analysis 27, 617–621.
Liang, G., Cai, S., Zhang, P., Peng, Y., Chen, H., Zhang, S., Kong, J., 2011. Anal. Chim. Acta 689, 243–249.
Lu, C., Yang, H., Zhu, C., Chen, X., Chen, G., 2009. Angew. Chem. Int. Edit. 48, 4785–4787.
Mak, A.C., Osterfeld, S.J., Yu, H., Wang, S.X., Davis, R.W., Jejelowo, O.A., Pourmand, N., 2010. Biosens. Bioelectron. 25, 1635–1639.
Miller, M.M., Prinz, G.A., Cheng, S.-F., Bounnak, S., 2002. Appl. Phys. Lett. 81, 2211.
Nierodzik, M.L., Karpatkin, S., 2006. Cancer Cell 10, 355–362.
Oh, S., Jadhav, M., Lim, J., Reddy, V., Kim, C.G., 2013. Biosens. Bioelectron. 41, 758–763.
Porfirieva, A., Evtugyn, G., Hianik, T., 2007. Electroanalysis 19, 1915–1920.
Qiu, H., Sun, Y., Huang, X., Qu, Y., 2010. Colloids Surf. B: Biointerfaces 79, 304–308.
Shimada, J., Maruyama, T., Kitaoka, M., Kamiya, N., Goto, M., 2012. Anal. Biochem. 421, 541–546.
Sinha, B., Anandakumar, S., Oh, S., Kim, C.G., 2012. Sens. Actuators A 182, 34–40.
Sinha, B., Hung, T.Q., Ramulu, T.S., Oh, S., Kim, K., Kim, D.-Y., Terki, F., Kim, C.G., 2013. J. Appl. Phys. 113, 063903.
Xu, Y., Yang, L., Ye, X., He, P., Fang, Y., 2006. Electroanalysis 18, 1449–1456.
Yang, H., Ji, J., Liu, Y., Kong, J., Liu, B., 2009. Electrochem. Commun. 11, 38–40.
Yang, H., Chen, L., Lei, C., Zhang, J., Li, D., Zhou, Z.-M., Bao, C.-C., Hu, H.-Y., Chen, X., Cui, F., Zhang, S.-X., Zhou, Y., Cui, D.-X., 2010. Appl. Phys. Lett. 97, 043702.
Yoon, J., Choi, N., Ko, J., Kim, K., Lee, S., Choo, J., 2013. Bios. Bioelectron. 47, 62–67.
Zhang, Y., Sun, X., 2011. Chem. Commun. 47, 3927–3929.